Electronic Supplementary Material (ESI) for Physical Chemistry Chemical Physics.

From Vibrational Spectroscopy and Quantum Tunnelling to Periodic Band Structures – a Self-Supervised, All-Purpose Neural Network Approach to General Quantum Problems

Jakob Gamper[a], *Florian Kluibenschedl*[a],

Alexander K. H. Weiss[b] *and Thomas S. Hofer*[a*]

[a]Theoretical Chemistry Division, Institute of General, Inorganic and Theoretical Chemistry

Center for Chemistry and Biomedicine

University of Innsbruck, Innrain 80-82, A-6020 Innsbruck, Austria

Tel.: +43-512-507-57111, Fax: +43-512-507-57199

[b]Research Institute for Biomedical Aging Research.

University of Innsbruck, Rennweg 10, A-6020 Innsbruck, Austria

September 26, 2022

*Corresponding author – E-Mail: t.hofer@uibk.ac.at

S.1 Supplement to Methods

S.1.1 Overlap Integral of Activation Functions

The overlap integral of two basis functions represents a key calculation step within the unsupervised learning process of the FF-ANN. This overlap integral describes the scalar product between two activation functions and is applied e.g. when determining the orthogonality contribution for the loss function. In the following derivation the activation function can be assumed to be located only in the real space without any loss of generality, hence no sub-layer $\mathcal{I}$ is considered:

$$\begin{aligned}
\langle \psi_1, \psi_2 \rangle &= \int_{x_{\min}}^{x_{\max}} \psi_1^* \cdot \psi_2 dx \\
&= \int_{x_{\min}}^{x_{\max}} \left(\sum_i^n a_{1,i} g_{1,i}(x) \right) \cdot \left(\sum_j^n a_{2,j} g_{2,j}(x) \right) dx \\
&= \int_{x_{\min}}^{x_{\max}} \sum_i^n \sum_j^n a_{1,i} g_{1,i}(x) a_{2,j} g_{2,j}(x) dx \\
&= \sum_i^n \sum_j^n a_{1,i} a_{2,j} \int_{x_{\min}}^{x_{\max}} g_{1,i}(x) g_{2,j}(x) dx
\end{aligned} \tag{S.1}$$

Considering the SIREN activation function, where $g(x) = sin(wx + b)$, the integral can be evaluated to following form

$$\begin{aligned}
\langle \psi_1^{\text{SIREN}}, \psi_2^{\text{SIREN}} \rangle &= \int_{x_{\min}}^{x_{\max}} \psi_1^{\text{SIREN}} \cdot \psi_2^{\text{SIREN}} dx \\
&= \sum_i^n \sum_j^n a_{1,i} a_{2,j} \int_{x_{\min}}^{x_{\max}} sin(w_{1,i} x + b_{1,i}) sin(w_{2,j} x + b_{2,j}) dx \\
&= \sum_i^n \sum_j^n a_{1,i} a_{2,j} \left[\frac{\sin\left((w_{2,j} - w_{1,i})\, x + b_{2,j} - b_{1,i} \right)}{2\,(w_{2,j} - w_{1,i})} \right]_{x_{min}}^{x_{max}} - \\
&\quad \sum_i^n \sum_j^n a_{1,i} a_{2,j} \left[\frac{\sin\left((w_{2,j} + w_{1,i})\, x + b_{2,j} + b_{1,i} \right)}{2\,(w_{2,j} + w_{1,i})} \right]_{x_{min}}^{x_{max}},
\end{aligned} \tag{S.2}$$

in contrast the integral over the Gaussian function can only be evaluated numerically,

$$
\begin{aligned}
\langle \psi_1^{\text{gaussian}}, \psi_2^{\text{gaussian}} \rangle &= \int_{x_{\min}}^{x_{\max}} \psi_1^{\text{gaussian}} \cdot \psi_2^{\text{gaussian}} dx \\
&= \sum_i^n \sum_j^n a_{1,i} a_{2,j} \int_{x_{\min}}^{x_{\max}} e^{-\left((w_{1,i}+w_{2,j})x^2 + b_{1,i} + b_{2,j}\right)} dx, \\
&= \sum_i^n \sum_j^n \frac{a_{1,i} a_{2,j} \sqrt{\pi}}{2\sqrt{w_{1,i}+w_{2,j}}} e^{-(b_{1,i}+b_{2,j})} \left[\operatorname{erf}\left(x\sqrt{w_{1,i}+w_{2,j}}\right)\right]_{x_{min}}^{x_{max}}
\end{aligned}
\tag{S.3}
$$

which corresponds to a summation over numerically computable Gaussian error functions.

S.1.2 Orthogonality Contribution

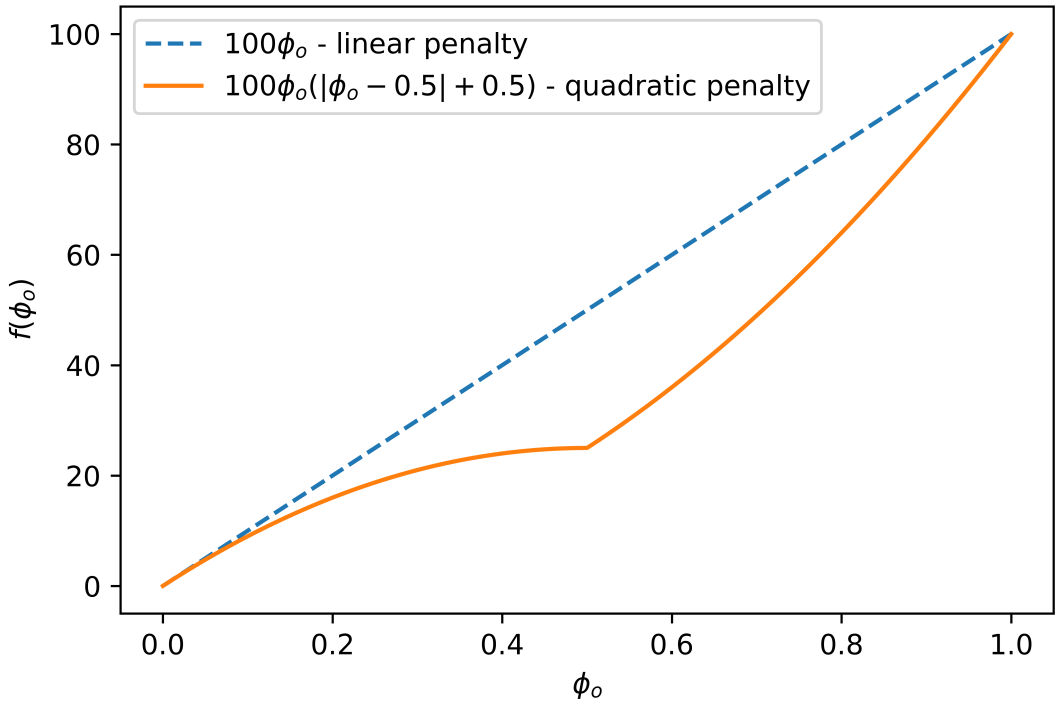

Fig. S.1: Comparison of a linear penalty (blue dashed) applied to the orthogonality with a quadratic-like penalty (orange). The figure highlights the steeper slope in the limit $\phi_o \to 1$ for the quadratic penalty, which results in a stronger repulsion from previously found states, especially in the beginning of the optimization.

S.2 Supplementary Results

S.2.1 Harmonic Oscillator and Morse Potential

Table S.1: Comparison of the 8 lowest analytic eigenenergies of a quantum harmonic oscillator ($\hbar = 1, \mu = 1, \omega = 1$) and the 6 lowest eigenergies of a Morse oscillator ($\hbar = 1, \mu = 1, a = 1.5, D_e = 20$ and $x_c = 0$) against the results obtained *via* the FF-ANN framework employing 40 and 65 neurons respectively. Energies are given in hartree.

n	E_n Harmonic		E_n Morse	
	Analytic	FF-ANN	Analytic	FF-ANN
0	0.5	0.5000000	4.1908859	4.1909034
1	1.5	1.5000003	10.8851578	10.8852722
2	2.5	2.5000013	15.3294296	15.3305088
3	3.5	3.5000045	17.5237025	17.5248299
4	4.5	4.5000541	17.8393715	17.8457102
5	5.5	5.5011938	18.0108957	18.0177432
6	6.5	6.4999631		
7	7.5	7.5002975		

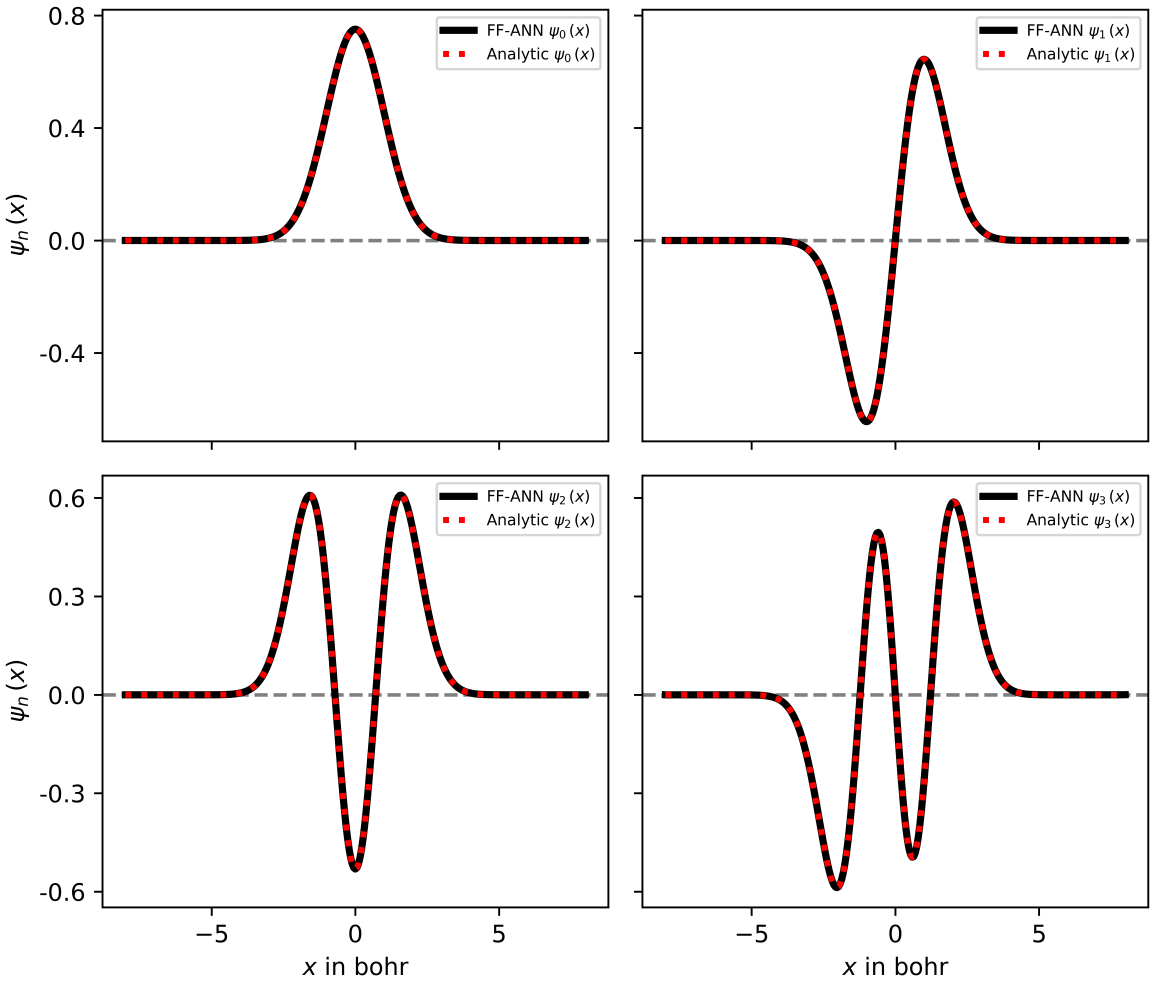

Fig. S.2: Comparison of the 4 lowest analytical eigenstates (red dashed) of a quantum harmonic oscillator (setting $\hbar = 1, \mu = 1$ and $\omega = 1$) with the results obtained *via* the FF-ANN approach (red dashed). The FF-ANN was built with 40 neurons.

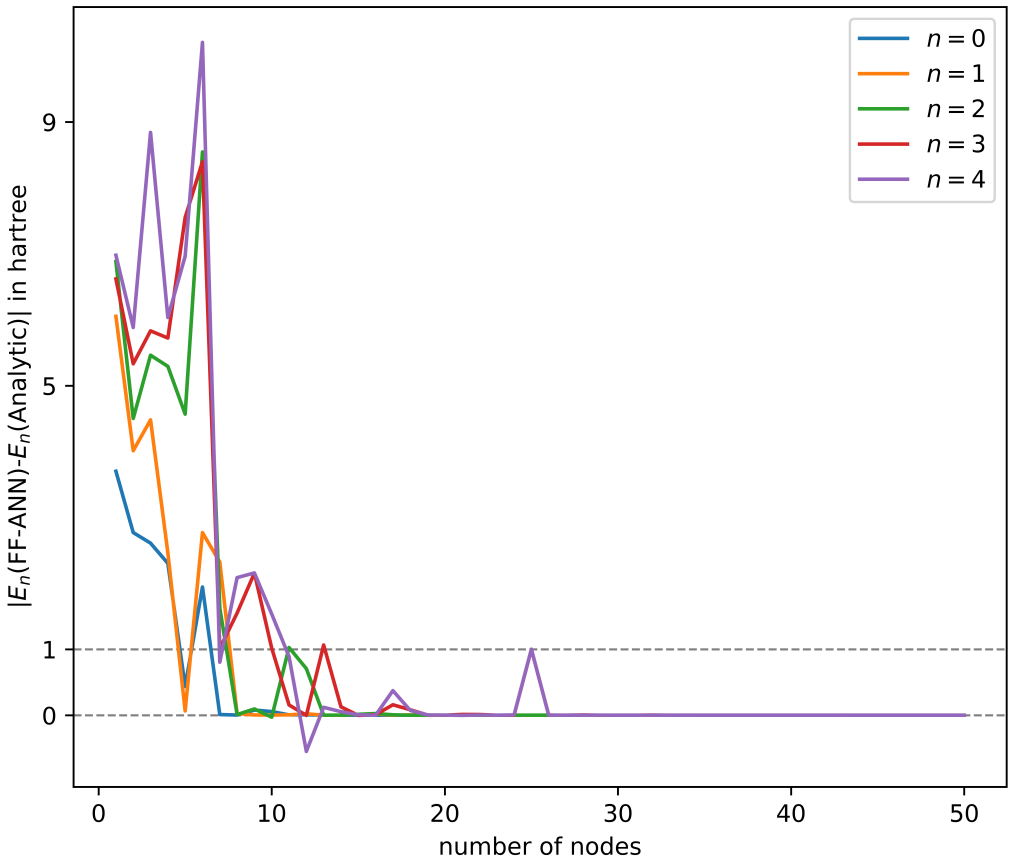

Fig. S.3: Results of the node scan for a quantum harmonic oscillator (setting $\hbar = 1, \mu = 1$ and $\omega = 1$). The difference between the FF-ANN and analytic eigenenergy for every state is plotted against the number of nodes. When employing 30+ neurons, the FF-ANN eigenenergies agree with their analytic counterparts to a high precision up to the 5-th eigenstate ($n = 4$).

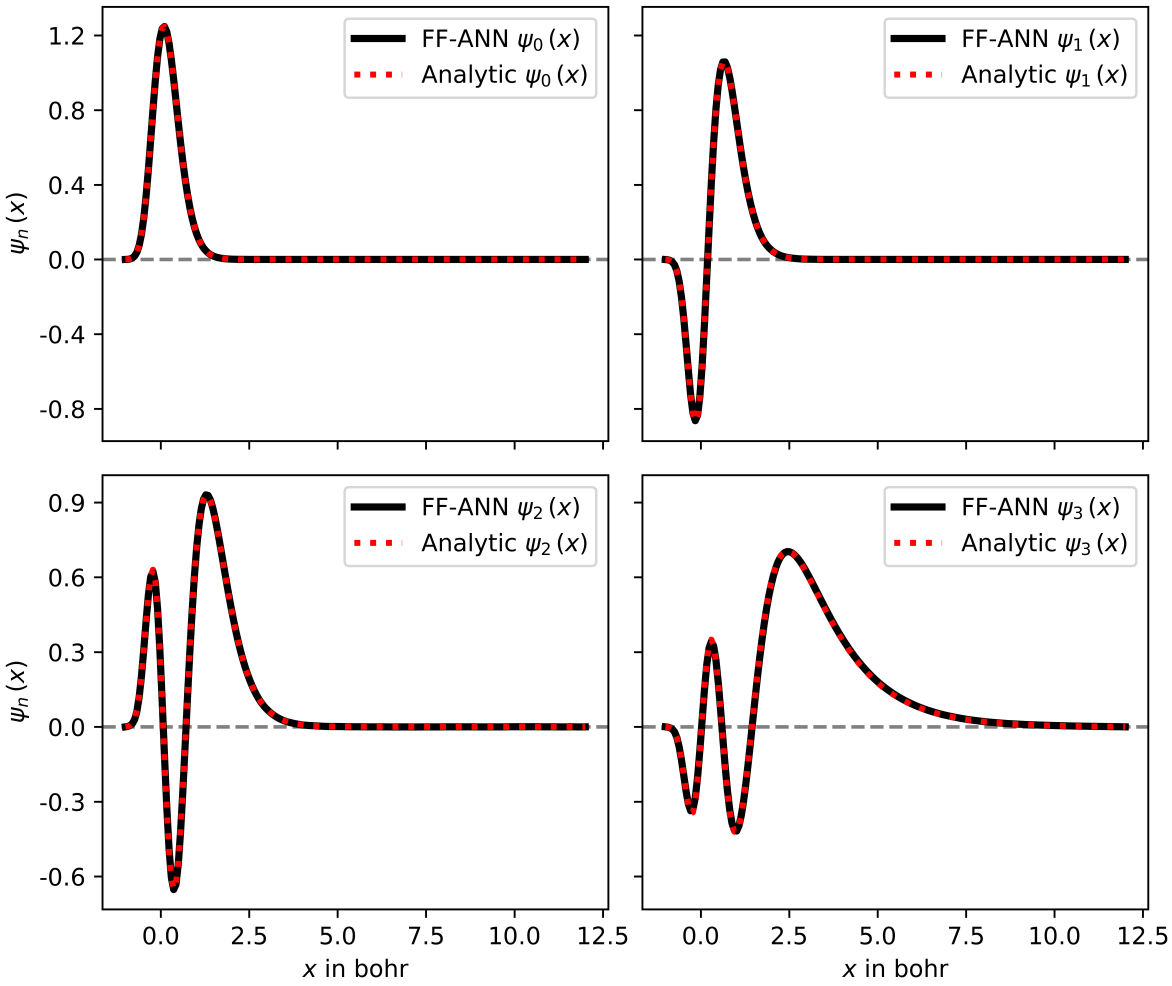

Fig. S.4: Comparison of the 4 lowest analytical eigenstates (red dashed) of a Morse oscillator (setting $\hbar = 1, \mu = 1, a = 1.5, D_e = 20$ and $x_c = 0$) with the results obtained *via* the FF-ANN approach (black). The FF-ANN was built with 65 neurons.

S.2.2 Rotational States of HCl^{35} Rigid Rotor

Table S.2: Comparison of the analytical transition wavenumbers of the 10 lowest rotational states of the HCl^{35} molecule as a rigid rotator against the results obtained *via* the FF-ANN framework employing 40 neurons. The analytical eigenenergies can be determined *via* $E = -\frac{\hbar^2}{2I}J(J+1)$ with J being the rotational angular momentum quantum number and $I = 1.597\,89\,\mathrm{g/mol\AA}^2$. Wavenumbers are given in cm^{-1}.

Transition	Analytic	FF-ANN	$\lvert\Delta\overline{\nu}\rvert$
0-1	10.549428168652	10.5494281686610	9E-12
1-2	31.648284505986	31.6482845059830	3E-12
2-3	52.747140843313	52.7471408433060	7E-12
3-4	73.845997180584	73.8459971806280	4.3E-11
5-6	94.944853518007	94.9448535179500	5.7E-11
6-7	116.043709855167	116.0437098552720	1.0E-10
7-8	137.142566184570	137.1425661925941	8.0E-9
8-9	158.241422507206	158.2414225299169	2.3E-8
9-10	179.340278798078	179.3402788672390	6.9E-8

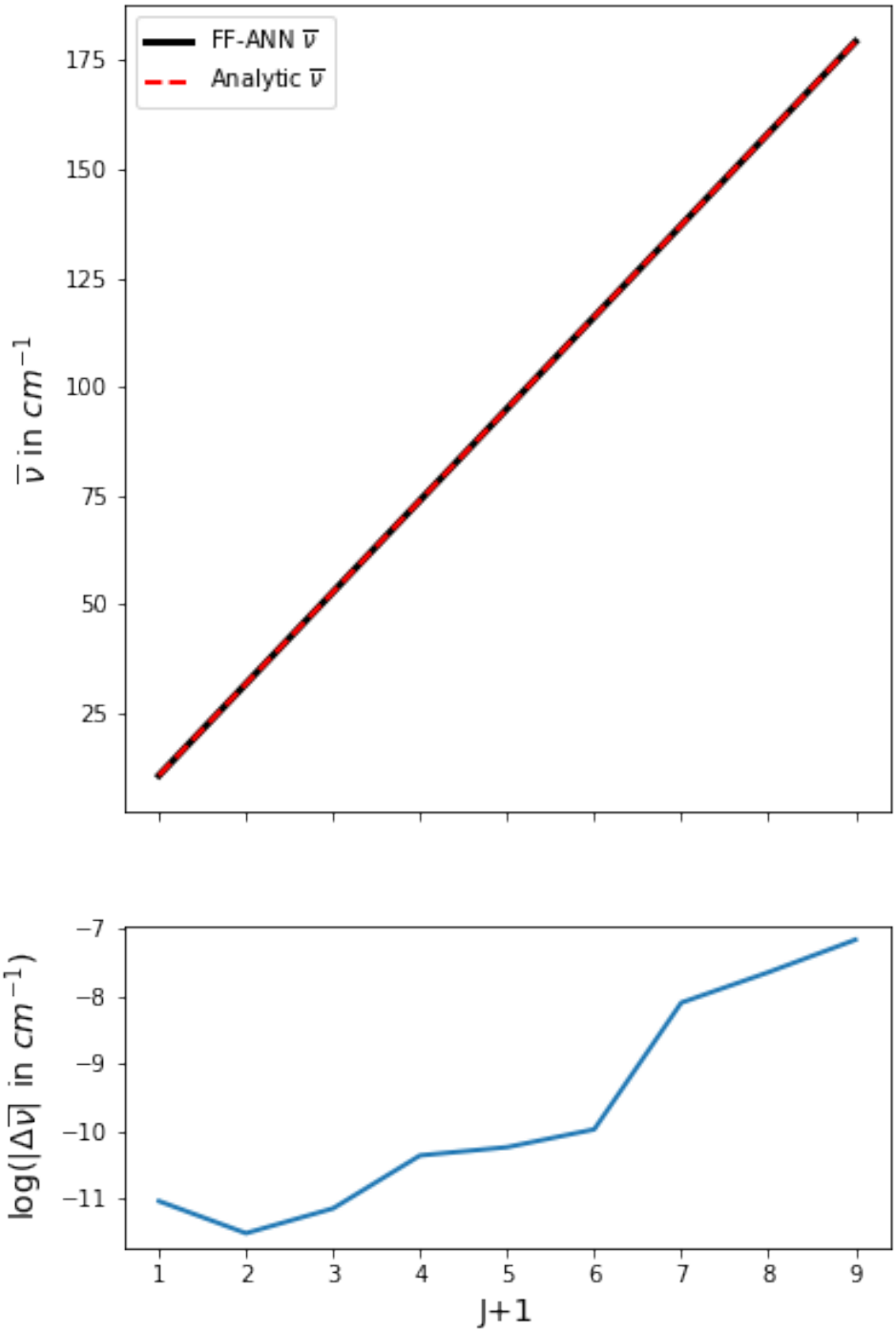

Fig. S.5: Comparison of the analytical transition wavenumbers of the 10 lowest rotational states of the HCl^{35} molecule as a rigid rotator against the results obtained *via* the FF-ANN framework employing 40 neurons. In the upper plot the rotational transitions of the FF-ANN and the analytical data are given. The lower plot represents the absolute deviations between the FF-ANN and the analytical solutions with a logarithmic scale.

S.2.3 Razavy and Hyperbolic Double Well Potential

Table S.3: Comparison of the analytical eigenenergies of the 7 lowest states for the hyperbolic and the Razavy double-well potentials as shown in figures S.6 and S.7 against the results obtained *via* the FF-ANN framework employing 55 and 65 neurons. Energies are given in hartree.

n	E_n Hyperbolic		E_n Razavy	
	Analytic	FF-ANN	Analytic	FF-ANN
0	3.6117753	3.6118140	15.6246588	15.6246606
1	3.6498299	3.6497912	15.6247205	15.6247245
2	9.8896220	9.8896221	43.2555013	43.2568218
3	10.7467599	10.7467599	43.2760513	43.2748418
4	14.9973344	14.9973344	64.4698618	64.4704945
5	18.2095036	18.2095036	65.7900215	65.7908659
6	22.4372499	22.4372499	77.8179335	77.8199832

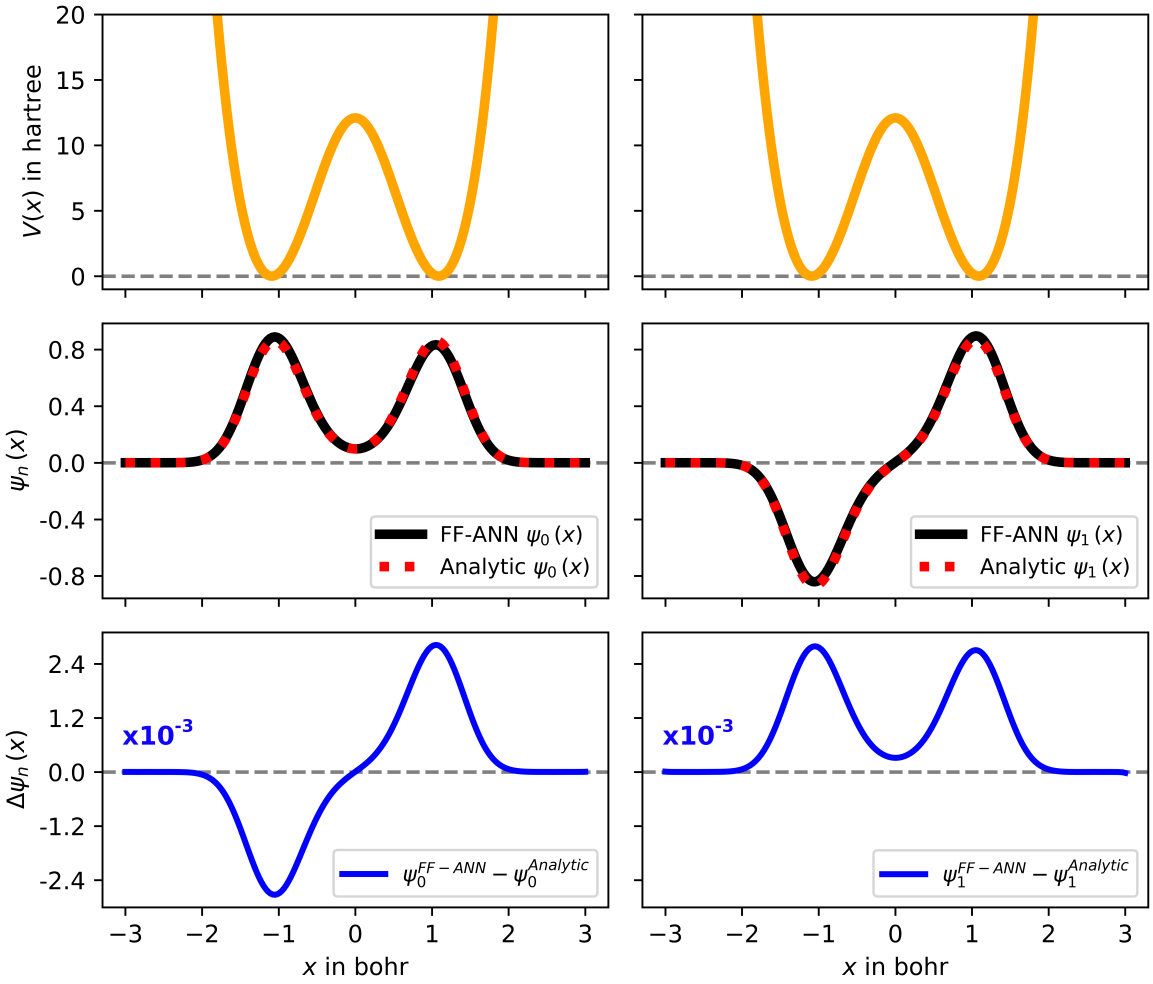

Fig. S.6: Hyperbolic double well potential (orange) with parameters $a = 2$ and $k = 30$ is shown on top. Again $\hbar = 1$ and $\mu = 1$. The wave functions of the symmetric ground and antisymmetric first excited state, obtained *via* a FF-ANN with 55 neurons (black) are depicted with their respective analytic counterparts (red dashed). The spatial differences (blue) between numerical and analytic wave functions are shown at the bottom and are of order 10^{-3}.

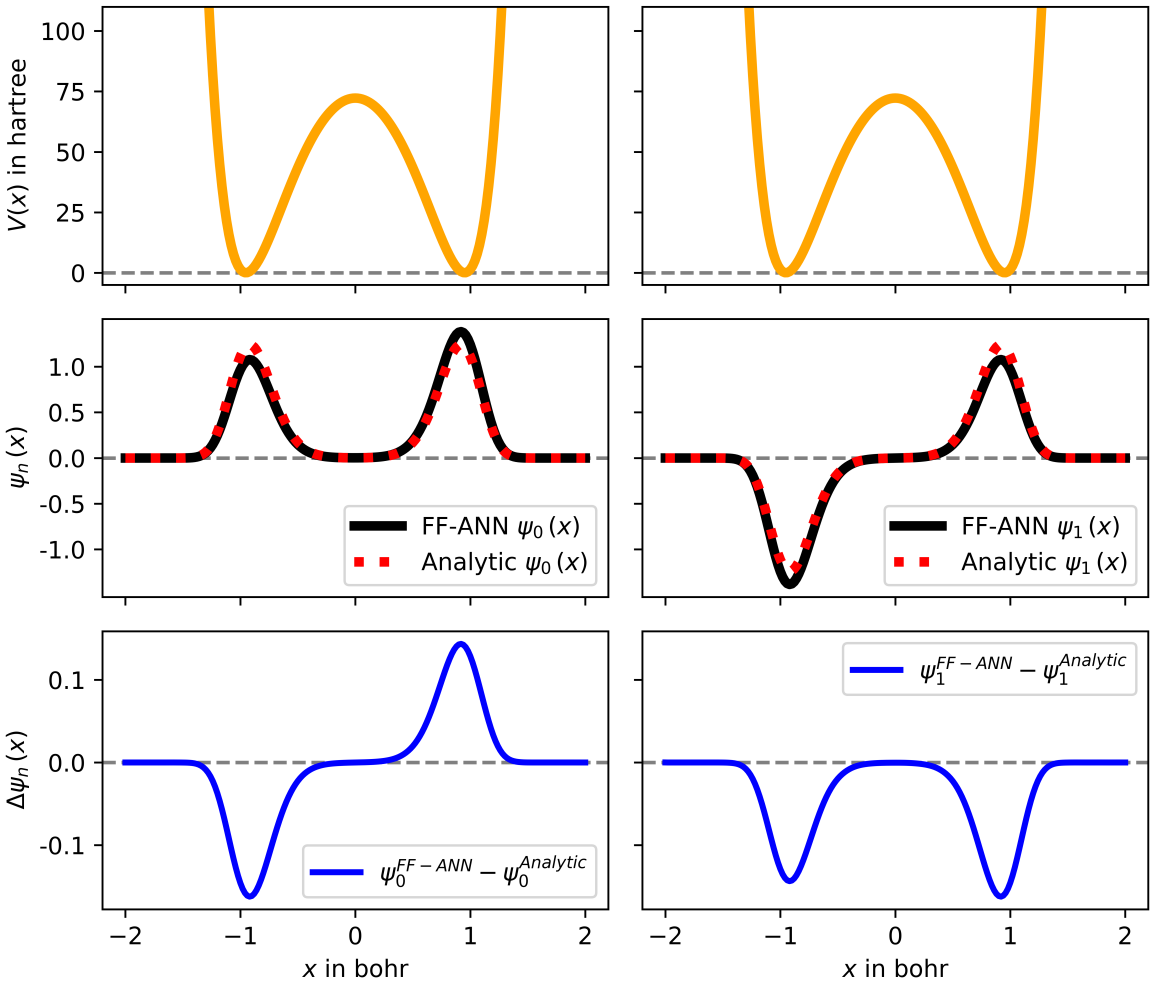

Fig. S.7: Razavy potential (orange9 with parameters $\xi = 3.5$ and $M = 12$ is shown on top. Again $\hbar = 1$ and $\mu = 1$. The wave functions of the symmetric ground and antisymmetric first excited state, obtained *via* a FF-ANN with 65 neurons (black) are depicted with their respective analytic counterparts (red dashed). The spatial differences (blue) between numerical and analytic wave functions are shown at the bottom.

S.2.4 Vibrations of H_2, HD and D_2

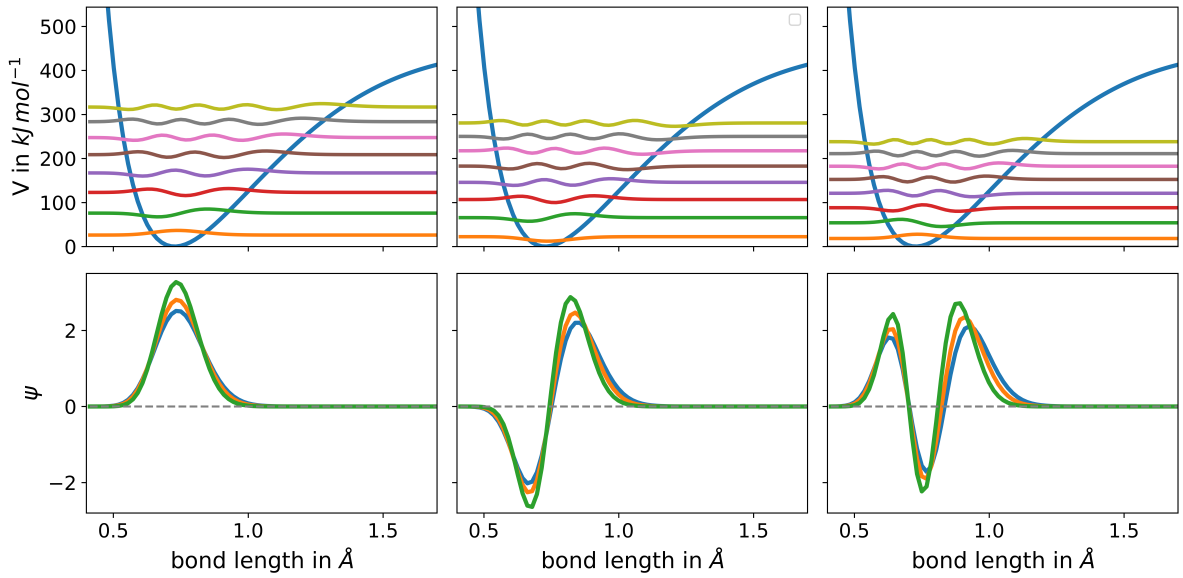

Fig. S.8: At the top from left to right the vibrational stretch poetential energies calculated at Full-CI/cc-pVQZ level, the ground state and the first seven excited states shifted with their respective eigenvalues of H_2, HD, and D_2 are shown. At the bottom the influence of the different effective masses on the first three eigenstates regarding the three isotopologues H_2 (blue), HD (orange) and D_2 (green) is pointed out *via* a graphical comparison. All eigenstates were obtained by the application of the FF-ANN on the generated PES using 40 nodes and the SIREN activation function approach.